Hindawi
Evidence-Based Complementary and Alternative Medicine
Volume 2019, Article ID 5475426, 13 pages
https://doi.org/10.1155/2019/5475426

Research Article

A Mathematical Model to Study the Mechanical Information Induced by Lifting-Thrusting Needle

Yi Yu, Wei Yao, and Guanghong Ding

Department of Aeronautics and Astronautics, Fudan University, Shanghai Research Center of Acupuncture, 220 Handan Road, Shanghai, 200433, China

Correspondence should be addressed to Wei Yao; weiyao@fudan.edu.cn

Received 25 October 2018; Revised 7 January 2019; Accepted 11 March 2019; Published 8 April 2019

Academic Editor: Jeng-Ren Duann

Focusing on the mechanical effect of traditional Chinese acupuncture, this study builds a mathematical model that simulates the mechanical process of lifting-thrusting needle. Analytic and numerical solutions are obtained to explore the mechanical information (displacement, strain, stress, and energy) in the skin tissue. Our results show that (1) needle manipulation leads to tissue displacement and mechanical stress field, but the needle should be inserted into the right position (about π/ω cm around the acupoint, where ω is the angular frequency) and enough depth (about 2 cm in lower limbs) to achieve effective mechanical stimuli; (2) the tissue displacement decays with an increase of distance from the stimulus position, more rapidly at higher frequencies; (3) there is an inverse relationship between the area of the 'effective influence region' (where shear strain > 0.2) and the stimulus frequency, which means larger needle movement is needed at higher frequencies to achieve a better curative effect; (4) more energy is required to maintain high frequency manipulation. This study proposes a preliminary comprehension of the mechanical response around the needle during the acupuncture process.

1. Introduction

Acupuncture, a physiotherapy sourced from Traditional Chinese Medicine (TCM), now gains recognition all around the world. Its therapeutic effect has been widely accepted since the National Institutes of Health Hearing in 1997 [1]. Acupuncture is a biomechanical process, during which a needle is inserted into the skin at the acupoint, and mechanical stimulation to the tissue is generated when twisting or lifting the needle. Elucidating the mechanical and biological mechanism of acupuncture effect is one of the urgent problems in TCM as well as international researches on physiotherapy.

The premise to accomplish acupuncture effect is to get sensations ("De Qi" in Chinese), which means to maintain a certain intensity of stimulation by manipulating the needle. However, "De Qi" is usually described subjectively according to the experiences of skillful acupuncturists and the feelings of some sensitive patients; the underlying issues are lack of quantitative research. Therefore, it is important to make clear the mechanical sensation in acupuncture and to reveal the key factors related to it.

Numerous work and different explanations have been put forward to help understand the acupuncture process. Recent morphological studies have made clear that the acupoint is mainly composed of connective tissue. As shown in Figure 1, the dermic dense connective tissue and subcutaneous loose connective tissue form a three-dimensional collagen fiber network with numerous intertwining blood vessels, nerves, mast cells, and lymphatic vessels [2, 3]. Goh et al. hypothesized that there might be a relationship between the efficacy of acupuncture treatment and the depth of insertion needle [4]. Langevin et al. hypothesized that needle manipulation generates mechanical signals at acupoints [5], where longitudinal waves and transverse waves can propagate. Acupuncture needle manipulation results in sustained stretching by lifting-thrusting or rotating in the tissue of the acupoint [6]. Yu et al.'s experiment showed that the acupuncture effect and the force on the needle are very significant when the collagen structure is complete, and when the collagen is destroyed, the

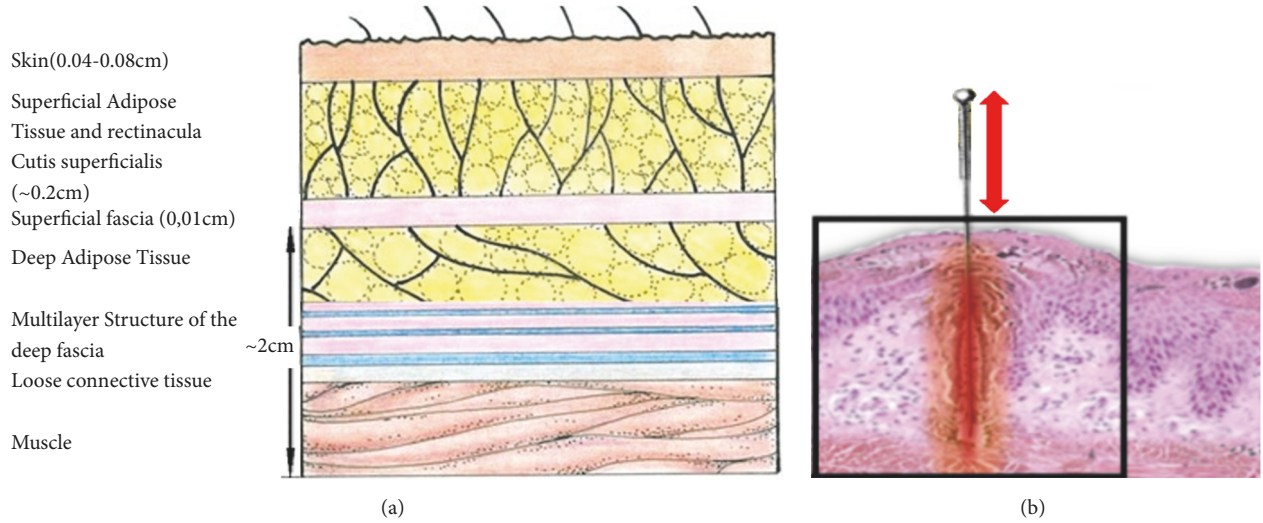

Figure 1: Acupoint morphology. (a) Basic pattern of organization of subcutaneous layers [9, 10]; (b) acupuncture location in lower limbs.

acupuncture effect is significantly weakened and the force on the needle body is very small [7]. Mvogo et al. constructed the analytic solutions of the tissue with collagen [8].

The mechanical effect of needle insertion and manipulation is the key to acupuncture; however, researches related with the quantitative mechanical effect of acupuncture are limited. Deleuze et al. has numerically simulated the features of subcutaneous interstitial flow induced by acupuncture [11]. Thiriet et al.'s mathematical model analyzed the different effects between acupuncture positioned at and out of acupoints [12]. We have also constructed a mathematical model to analyze the needle rotation at acupoints [13]. In this study, the previous work is extended, and the acupuncture of lifting-thrusting manipulation is studied through the establishment of a mechanical model based on the theory of viscoelastic mechanics. The influences of needle factors, such as stimulus frequency, movement amplitude, radius, and insertion depth, have been discussed in order to explore the acupuncture mechanical effect.

2. Methods

2.1. Model. Soft tissues are usually assumed as viscoelastic materials; some are more "elastic" and some are more "viscous"; they exhibit obvious hysteresis, stress relaxation, and other viscoelastic phenomena [14]. In our model, the skin tissue is treated as a semi-infinite viscoelastic body and the needle is treated as a rigid body. As shown in Figure 2, the tissue is divided into two parts. Part (1) represents the tissue from the plane of the tip location to infinity ($z \geq 0$) where tissue displacement is caused by the movement of the needle tip (point A). Part (2) is the needle manipulation region ($-L_0 \leq z < 0$), where L_0 is the needle insertion depth and the standard L_0 is 2 cm in lower limbs.

2.2. Equations. The soft tissue is supposed as a homogeneous isotropic incompressible viscoelastic body and fit for Feng's quasilinear viscoelastic theory of small amplitude displacement [15]. For acupuncture manipulation, the needle movement causes small amplitude oscillatory displacements in the low stress range (physiological state) of the tissue. The boundary conditions are specified as simple harmonic functions of time; therefore, the variables can be expressed as

$$\begin{aligned} u_i(x_i,t) &= \widetilde{u}_i e^{i\omega t} \\ \sigma_{ij}(x_i,t) &= \widetilde{\sigma}_{ij} e^{i\omega t} \\ \varepsilon_{ij}(x_i,t) &= \widetilde{\varepsilon}_{ij} e^{i\omega t} \\ &\quad (i,j=1,2,3). \end{aligned} \tag{1}$$

where u_i is the displacement component which is the distance from the original (equilibrium) position, x_i is the coordinate component, t is the time, ω is the angular frequency, σ_{ij} is the component of stress tensor, and ε_{ij} is the component of strain tensor.

Based on the strain-displacement relation and excluding the effect of volume force, we get the governing equation of motion in linear viscoelastic medium

$$\left[\lambda^*(i\omega) + \mu^*(i\omega)\right] du_{j,ji} + \mu^*(i\omega)\, du_{i,jj} = \rho \frac{\partial^2 u_i}{\partial t^2}. \tag{2}$$

where $\mu^*(i\omega)$ and $\lambda^*(i\omega)$ are the viscoelastic material parameters and ρ is the density. Postulate the tissue is incompressible, that is, $u_{j,ji} = 0$, and putting (1) into (2), we get

$$\mu^*(i\omega)\, d\widetilde{u}_{i,jj} = -\rho\omega^2 \widetilde{u}_i \tag{3}$$

Rewrite it in tensor form

$$\mu^*(i\omega)\, \nabla^2 \overrightarrow{\widetilde{u}} = -\rho\omega^2 \overrightarrow{\widetilde{u}} \tag{4}$$

Suppose the tissue around the needle is a semi-infinite space. This is an axisymmetric problem ($u_\theta = 0, \partial/\partial\theta = 0$). Replace

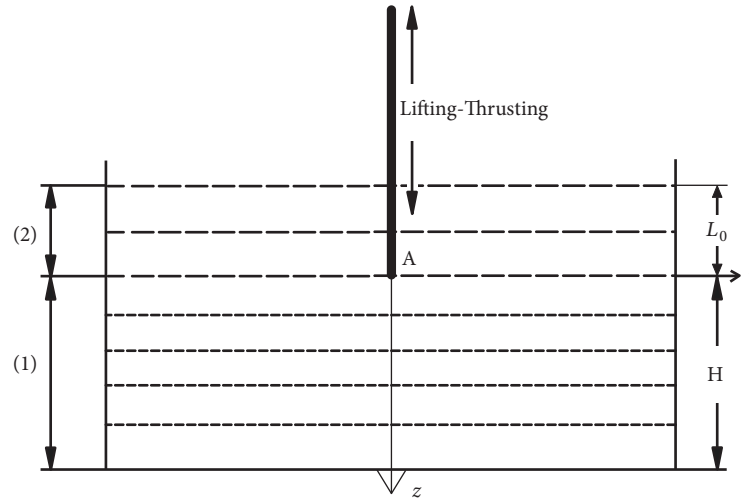

Figure 2: Diagrammatic sketch of lifting-thrusting manipulation.

μ^* with μ and $\tilde{u}$ with u; then we have (5) in cylindrical coordinate

$$\mu\left(\frac{\partial^2 u_r}{\partial r^2}+\frac{1}{r}\frac{\partial u_r}{\partial r}-\frac{u_r}{r^2}+\frac{\partial^2 u_r}{\partial z^2}\right)=-\rho\omega^2 u_r$$
$$\mu\left(\frac{\partial^2 u_z}{\partial r^2}+\frac{1}{r}\frac{\partial u_z}{\partial r}+\frac{\partial^2 u_z}{\partial z^2}\right)=-\rho\omega^2 u_z. \tag{5}$$

where u_r and u_z are the displacement amplitude in r and z direction, respectively. Defining the dimensionless parameters: $U_Z = u_z/u_0, U_R = u_r/u_0, Z = z/u_0, R = r/u_0$, where u_0 is the amplitude of needle movement. Then (5) is changed to

$$\mu\left(\frac{\partial^2 U_R}{\partial R^2}+\frac{1}{R}\frac{\partial U_R}{\partial R}-\frac{U_R}{R^2}+\frac{\partial^2 U_R}{\partial Z^2}\right)=-\rho\omega^2 {u_0}^2 U_R \tag{6a}$$
$$\mu\left(\frac{\partial^2 U_Z}{\partial R^2}+\frac{1}{R}\frac{\partial U_Z}{\partial R}+\frac{\partial^2 U_Z}{\partial Z^2}\right)=-\rho\omega^2 {u_0}^2 U_Z. \tag{6b}$$

Based on the strain-displacement relation

$$\varepsilon_{rz}=\frac{1}{2}\left(\frac{\partial u_z}{\partial r}+\frac{\partial u_r}{\partial z}\right)e^{i\omega t}=\frac{1}{2}\left(\frac{\partial U_Z}{\partial R}+\frac{\partial U_R}{\partial Z}\right)e^{i\omega t}$$
$$=E_{RZ}e^{i\omega t}. \tag{7}$$

where E_{RZ} is calculated by explicit difference scheme

$$E_{RZ}=\frac{1}{2}\left(\frac{\partial U_Z}{\partial R}+\frac{\partial U_R}{\partial Z}\right)$$
$$\approx\frac{1}{2\Delta R}\left(U_{Zj+1,k}-U_{Zj,k}\right)+\frac{1}{2\Delta Z}\left(U_{Rj,k+1}-U_{Rj,k}\right). \tag{8}$$

And the corresponding stress is

$$\begin{aligned}\tau_{rz}&=\mathrm{Re}\left\{2\mu\left(i\omega\right)\varepsilon_{rz}\right\}\\&=\mathrm{Re}\left\{\left(\mu_1+i\mu_2\right)\cdot 2E_{RZ}\left[\cos\left(\omega t\right)+i\sin\left(\omega t\right)\right]\right\}\\&=2E_{RZ}\left[\mu_1\cos\left(\omega t\right)-\mu_2\sin\left(\omega t\right)\right]\\&=2E_{RZ}\left|\mu\right|\cos\left(\omega t+\delta\right).\end{aligned} \tag{9}$$

where $|\mu| = \sqrt{\mu_1^2+\mu_2^2}$, $\tan\delta = \mu_2/\mu_1$, and δ is the phase difference between stress and strain. The shear stress amplitude $T_{RZ} = 2|\mu|E_{RZ}$.

In a cycle, the energy dissipation of one-unit volume caused by lifting-thrusting is

$$\begin{aligned}\Delta E&=\int_0^{2\pi/\omega}\tau_{rz}\dot{\varepsilon}_{rz}dt=4\left|\mu\right|\\&\cdot {E_{RZ}}^2\int_0^{2\pi/\omega}-\omega\left[\mu_1\cos\left(\omega t\right)-\mu_2\sin\left(\omega t\right)\right]\\&\cdot\sin\left(\omega t\right)dt=4\pi {E_{RZ}}^2\mu_2.\end{aligned} \tag{10}$$

The energy dissipation of the whole domain is

$$\begin{aligned}E_f&=\int_{r_0/u_0}^{+\infty}\int_{-L_0/u_0}^{+\infty}\Delta E dZ dR\\&=\int_{r_0/u_0}^{+\infty}\int_{-L_0/u_0}^{+\infty}4\pi\mu_2 {E_{RZ}}^2 dZ dR.\end{aligned} \tag{11}$$

Define $E_{\max}$ as the max energy stored

$$\begin{aligned}E_{\max}&=4\pi {E_{RZ}}^2\int_0^{\pi/\omega}\mu_1\omega\cos\left(\omega t\right)\sin\left(\omega t\right)dt\\&=2\pi\mu_1 {E_{RZ}}^2.\end{aligned} \tag{12}$$

Therefore, the mechanical quality factor Q which reflect the ratio of energy storage to energy dissipation is

$$Q = \frac{2\pi E_{\max}}{\Delta E} = \frac{\mu_1}{\mu_2}. \tag{13}$$

2.3. Boundary Conditions. The motion of the boundary is

$$\begin{aligned} &u_r = 0, \\ &u_z = u_0 \cos(\omega t) \\ &\qquad r = r_0, \ -L_0 \le z \le 0 \\ &u_r = u_z = 0 \quad z \longrightarrow \infty \\ &u_z = 0 \quad r \longrightarrow \infty, \end{aligned} \tag{14}$$

where r_0 is the radius of the needle. Then

$$\begin{aligned} &U_R = 0 \quad R \longrightarrow 0 \cup R \longrightarrow \infty \cup Z \longrightarrow \infty \\ &U_Z = 0 \quad R \longrightarrow \infty \cup Z \longrightarrow \infty \\ &U_Z = 1 \quad R \longrightarrow 0 \cap -\frac{L_0}{u_0} \le Z \le 0. \end{aligned} \tag{15}$$

2.4. Analytic Solutions of Part (1). Let $U_R = F(R)G(Z)$; (6a) is expressed as

$$\frac{F_{RR} + (1/R)F_R - \left(1/R^2\right)F}{F} + \frac{G_{ZZ}}{G} + \frac{\rho\omega^2 {u_0}^2}{\mu} = 0. \tag{16}$$

Let $G_{ZZ}/G = \lambda$; then we get

$$G_{ZZ} - \lambda G = 0 \tag{17a}$$

$$R^2 F_{RR} + RF_R + \left[\left(\frac{\rho\omega^2 {u_0}^2}{\mu} + \lambda\right)R^2 - 1\right]F = 0. \tag{17b}$$

Equation (17b) is a 1-order Bessel equation, and the solutions are

$$\begin{aligned} G(Z) &= A_1 e^{\sqrt{\lambda}Z} + A_2 e^{-\sqrt{\lambda}Z} \\ F(R) &= B_1 J_1\left(\sqrt{\frac{\rho\omega^2 {u_0}^2}{\mu} + \lambda}R\right) \\ &\quad + B_2 Y_1\left(\sqrt{\frac{\rho\omega^2 {u_0}^2}{\mu} + \lambda}R\right), \end{aligned} \tag{18}$$

where J_1, Y_1 are 1-order Bessel function and Neumann function, respectively.

Inputting $U_R(Z \longrightarrow \infty) = 0$, we get $A_1 = 0$. Because $J_1(0) = 0$ and $Y_1(0) = -\infty$, based on the boundary condition $U_R(R \longrightarrow 0, Z = 0) = 0$, we get $B_2 = 0$; therefore

$$U_R = AJ_1\left(\sqrt{\frac{\rho\omega^2 {u_0}^2}{\mu} + \lambda}R\right)e^{-\sqrt{\lambda}Z}. \tag{19}$$

Because $J_1(+\infty) = 0$, then $U_R(R \longrightarrow \infty) = 0$.

Put $U_Z = F(R)G(Z)$ into (6b),

$$\frac{F_{RR} + (1/R)F_R}{F} + \frac{\rho\omega^2 {u_0}^2}{\mu} + \frac{G_{ZZ}}{G} = 0. \tag{20}$$

Let $G_{ZZ}/G = \lambda$; then we get

$$G_{ZZ} - \lambda G = 0 \tag{21a}$$

$$F_{RR} + \frac{1}{R}F_R + \left(\frac{\rho\omega^2 {u_0}^2}{\mu} + \lambda\right)F = 0. \tag{21b}$$

Equation (21b) is a 0-order Bessel equation; therefore the solutions are

$$\begin{aligned} G(Z) &= A_1 e^{\sqrt{\lambda}Z} + A_2 e^{-\sqrt{\lambda}Z} \\ F(R) &= B_1 J_0\left(\sqrt{\frac{\rho\omega^2 {u_0}^2}{\mu} + \lambda}R\right) \\ &\quad + B_2 Y_0\left(\sqrt{\frac{\rho\omega^2 {u_0}^2}{\mu} + \lambda}R\right). \end{aligned} \tag{22}$$

Inputting $U_z(Z \longrightarrow \infty) = 0$, we get $A_1 = 0$. Because $J_0(0) = 1$ and $Y_1(0) = -\infty$, based on the boundary condition $U_z(R \longrightarrow 0, Z = 0) = 1$, we get $B_2 = 0$; therefore

$$U_Z = J_0\left(\sqrt{\frac{\rho\omega^2 {u_0}^2}{\mu} + \lambda}R\right)e^{-\sqrt{\lambda}Z}. \tag{23}$$

Suppose the tissue is incompressible, that is, $\nabla \bullet \vec{v} = 0$; therefore

$$\frac{\partial U_R}{\partial R} + \frac{U_R}{R} + \frac{\partial U_Z}{\partial Z} = 0. \tag{24}$$

Putting (19) and (23) into (24), we get

$$\begin{aligned} &A\frac{\partial J_1\left(\sqrt{\rho\omega^2 {u_0}^2/\mu + \lambda}R\right)}{\partial R} \\ &\quad + A\frac{J_1\left(\sqrt{\rho\omega^2 {u_0}^2/\mu + \lambda}R\right)}{R} \\ &\quad - \sqrt{\lambda}J_0\left(\sqrt{\frac{\rho\omega^2 {u_0}^2}{\mu} + \lambda}R\right) = 0. \end{aligned} \tag{25}$$

Based on the recurrence relation of Bessel's function

$$\begin{aligned} J_{\nu-1}(x) + J_{\nu+1}(x) &= \frac{2\nu}{x}J_\nu(x) \\ J_{\nu-1}(x) - J_{\nu+1}(x) &= 2J'_\nu(x), \end{aligned} \tag{26}$$

we get

$$\frac{\partial J_1(kR)}{\partial R} = k\frac{J_0(kR) - J_2(kR)}{2}$$
$$\frac{J_1(kR)}{R} = k\frac{J_0(kR) + J_2(kR)}{2} \quad \left(k = \sqrt{\frac{\rho\omega^2 {u_0}^2}{\mu} + \lambda}\right). \tag{27}$$

Putting (27) into (25), we get

$$Ak\left(\frac{J_0(kR) - J_2(kR)}{2} + \frac{J_0(kR) + J_2(kR)}{2}\right) - \sqrt{\lambda}J_0(kR) = 0, \tag{28}$$

and then $A = \sqrt{\lambda}/k$. Therefore

$$U_Z = J_0\left(\sqrt{\frac{\rho\omega^2 {u_0}^2}{\mu} + \lambda}R\right)e^{-\sqrt{\lambda}Z}$$
$$U_R = \frac{\sqrt{\lambda}}{\sqrt{\rho\omega^2 {u_0}^2/\mu + \lambda}}J_1\left(\sqrt{\frac{\rho\omega^2 {u_0}^2}{\mu} + \lambda}R\right)e^{-\sqrt{\lambda}Z}. \tag{29}$$

2.5. Calculation Solutions of Part (2). Wang et al. have simplified the tissue as one-dimensional question [15]; therefore (6a) and (6b) is changed to

$$\mu\left(\frac{\partial^2 U_R}{\partial R^2} + \frac{1}{R}\frac{\partial U_R}{\partial R} - \frac{U_R}{R^2}\right) = -\rho\omega^2 {u_0}^2 U_R$$
$$\mu\left(\frac{\partial^2 U_Z}{\partial R^2} + \frac{1}{R}\frac{\partial U_Z}{\partial R}\right) = -\rho\omega^2 {u_0}^2 U_Z. \tag{30}$$

Based on $\nabla \bullet \vec{v} = 0$, the solutions are

$$U_R = 0$$
$$U_Z = J_0\left(\sqrt{\frac{\rho\omega^2 {u_0}^2}{\mu}}R\right). \tag{31}$$

Both (29) and (31) do not fit very much in this part; therefore, we suppose (31) as the upper boundary condition ($Z = -L_0/u_0$), (29) works as the lower boundary condition ($Z = 0$), linear interpolation is adopted to calculate part (2), that is,

$$U_R(R, Z) = -ZU_R(R, 0)$$
$$U_z(R, Z) = U_z(R, 0) + Z\left[U_z(R, 0) - U_z\left(R, -\frac{L_0}{u_0}\right)\right] \quad \left(-\frac{L_0}{u_0} < Z < 0\right). \tag{32}$$

2.6. Parameters. The analytic solution (29) shows that λ affects the amplitude attenuation along z. Langevin et al.'s research on acupuncture demonstrates the displacement is small when z is over 2 cm [10]. Therefore, we suppose the displacement amplitude at $z = 2$ cm is a small amount compared to the amplitude at $z = 0$ cm (the plane of the needle tip), that is $e^{-\sqrt{\lambda}(z/u_0)} \approx 10\%$; we can determine $\lambda \approx 0.25$. The standard u_0 is 0.5 cm and r_0 is 0.02 cm.

The biological viscoelasticity is determined by [16]

$$\mu(i\omega) = \frac{1 + (c/2)\left[\ln\left(1 + \omega^2\tau_2^2\right) - \ln\left(1 + \omega^2\tau_1^2\right)\right] + ic\left[\tan^{-1}(\omega\tau_2) - \tan^{-1}(\omega\tau_1)\right]}{1 + c\ln(\tau_2/\tau_1)}. \tag{33}$$

where $\tau_1 = 0.0984, \tau_2 = 8454.76, c = 0.0351$.

$J_0(\sqrt{\rho\omega^2 {u_0}^2/\mu + \lambda}R)$ and $J_1(\sqrt{\rho\omega^2 {u_0}^2/\mu + \lambda}R)$ will diverge at $R \longrightarrow \infty$ if $\rho\omega^2 {u_0}^2/\mu + \lambda$ have an imaginary part. Obviously, λ>0; notice that the imaginary part of $\rho\omega^2 {u_0}^2/\mu$ is small compared to the real part; for example, $\rho\omega^2 {u_0}^2/\mu = 1.2 - 0.03i$ when ω=2π and $\rho\omega^2 {u_0}^2/\mu$= 76 − 0.38i when ω=16π; therefore we replace $\sqrt{\rho\omega^2 {u_0}^2/\mu + \lambda}$ with its module $|\sqrt{\rho\omega^2 {u_0}^2/\mu + \lambda}|$ to void divergence.

3. Results

3.1. Boundary ($Z = 0, Z = -L_0/u_0$) Solutions. Obviously, the upper ($Z = -L_0/u_0$) and lower ($Z = 0$) boundary solutions determine displacement distributions in the skin tissue. The dimensionless tissue displacements (U_Z at the upper and lower boundaries and the U_R at the lower boundary) at two stimuli frequencies ($\omega = 2\pi$ and $\omega = 16\pi$) are plotted in Figure 3. The distributions of U_Z are very similar at upper and lower boundaries.

Figure 4 shows the corresponding absolute values of displacements ($|U_R|$ and $|U_Z|$) at lower boundary ($Z = 0$). Additionally, the combined displacement $U = \sqrt{U_R^2 + U_Z^2}$ is plotted. It shows that U is nearly the same as $|U_Z|$ and $|U_R|$ is relatively small, especially at high stimulus frequency (ω=16π, in Figure 4(b)). Therefore, we will only study U afterwards. The influence of stimulus frequency on the displacement (U) is shown in Figure 5. It is clear that U decreases with the increase of R, and at higher frequencies, it decreases more rapidly.

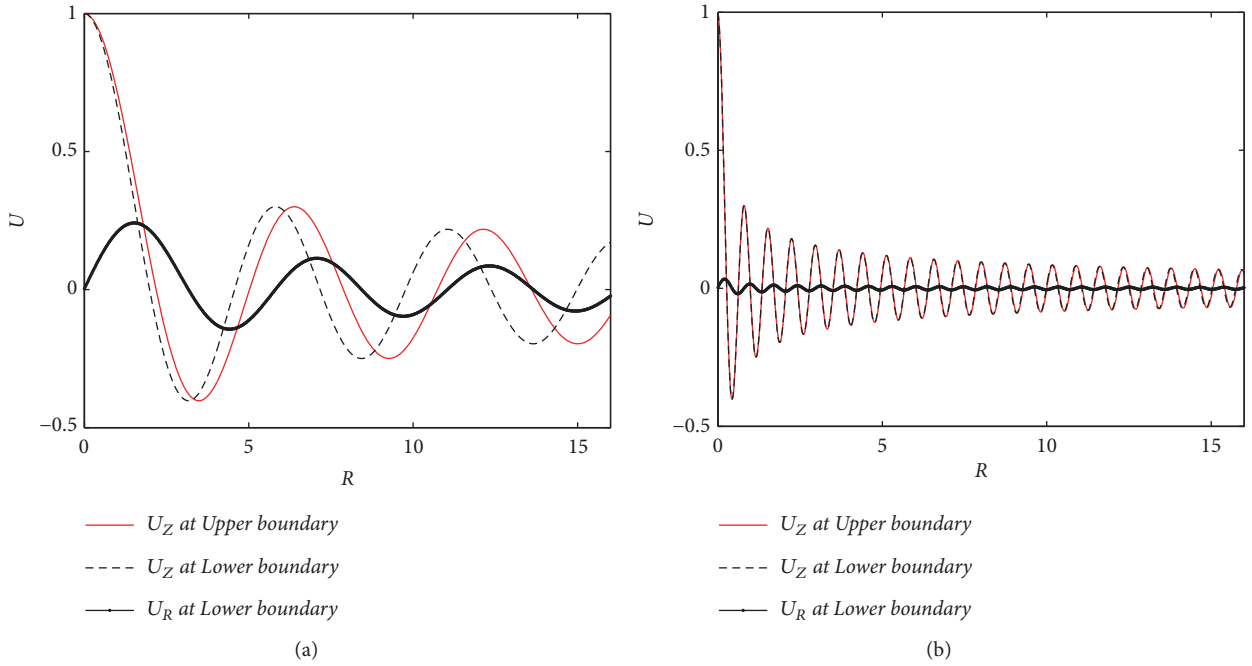

Figure 3: Amplitudes of tissue displacements at the upper ($Z = -L_0/u_0$) and lower ($Z = 0$) boundaries. (a) $\omega = 2\pi$; (b) $\omega = 16\pi$.

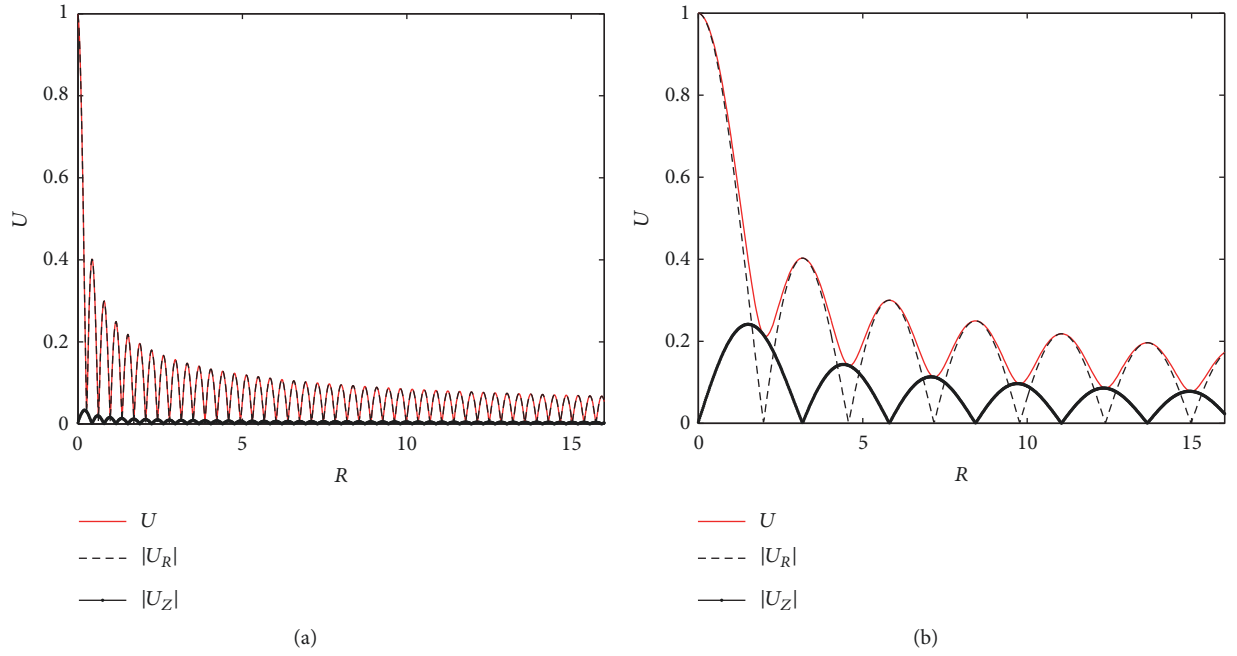

Figure 4: Amplitudes of tissue displacements at $Z = 0$. (a) $\omega = 2\pi$; (b) $\omega = 16\pi$.

The influence of needle movement amplitude (u_0) is shown in Figure 6. Figure 6(a) plots the absolute values of tissue displacement ($|u|$) at the lower boundary with different u_0s (0.25, 0.5, 0.75, and 1.0cm). The range of $|u|$ is largely dependent on u_0, with a nearly linear relationship at $R \longrightarrow 0$. Figure 6(b) shows the dimensionless displacement $U = |u|/u_0$, which attenuates a little more slowly along R direction with an increasing u_0. Figure 7 demonstrates U in the cases of different needle radius (r_0). It shows that r_0 has a minimal effect on U.

3.2. Displacement Amplitude (U) Distribution in the Skin Tissue. Figure 8 shows the displacement amplitude U distribution at $\omega = 2\pi$ and $\omega = 16\pi$. Comparing Figures 8(a) and 8(b) shows that the tissue displacement around the needle

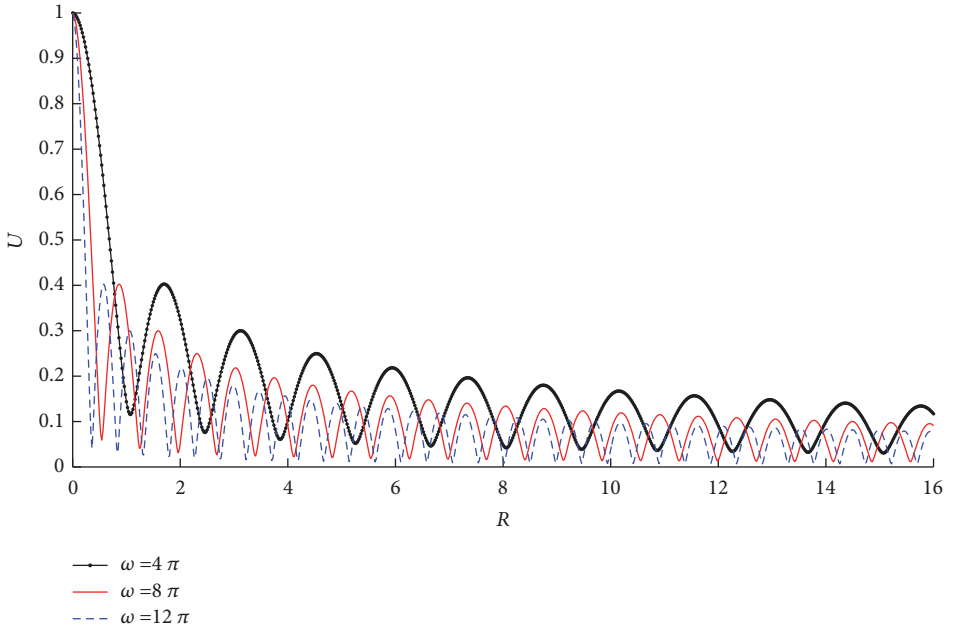

Figure 5: Amplitudes of tissue displacements under different frequencies.

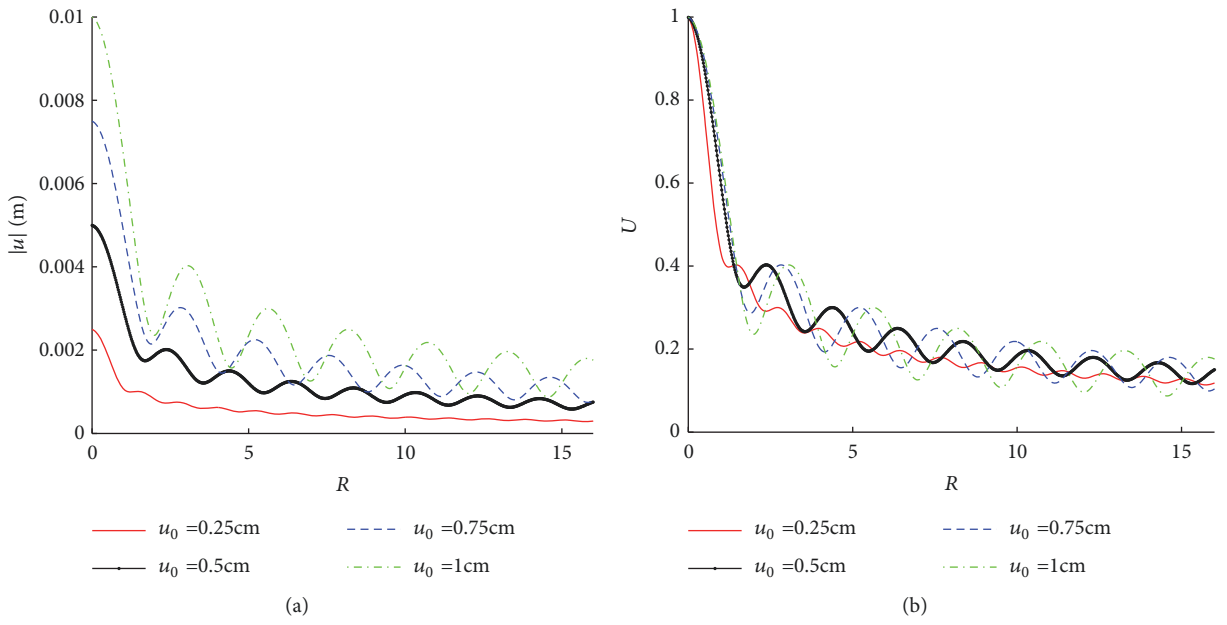

Figure 6: Amplitudes of tissue displacements under different u_0s at $\omega = 2\pi$; (a) $|u|$. (b) U.

($-L_0/u_0 \leq Z \leq 0$) decays along the radial direction R under both low and high frequency stimulus, but U decays less rapidly under low frequency ($U \leq 50\%$ where $r > 0.6$ cm) than that under high frequency ($U \leq 50\%$ where $r > 0.07$ cm). Moreover, U also decays quickly under the needle tip ($Z > 0$).

3.3. Shear Strains (ε_{rz}) and Stresses (τ_{rz}) under Different Frequencies. Figure 9 shows the contour lines of shear strain amplitude in absolute values ($|E_{RZ}|$) in the tissue. The needle is located at $R = 0$, $-4 \leq Z \leq 0$ (shown as white lines in Figure 9). The maximum shear strain occurs at the needle tip, and again, strains decay along the radial direction, with more rapid attenuation under high frequency stimulus. Thus, the low frequency stimulus affects larger area than high frequency stimulus. Take the area where $|E_{RZ}| > 0.2$ as the effective influence region S_{eff}, and define Z and R at $|E_{RZ}| \approx 0.2$ as Z_{thr} and R_{thr}, respectively; then $S_{\text{eff}} = Z_{\text{thr}} \times R_{\text{thr}} \approx 1 \times 0.94$ at $\omega = 2\pi$ and $S_{\text{eff}} \approx 1 \times 0.08$ at $\omega = 16\pi$, shown as the black rectangles in Figure 9. It turns out that the stimulus frequency has little effect on Z_{thr} but has significant influence on R_{thr}. Figure 10 shows the contour lines of dimensionless shear

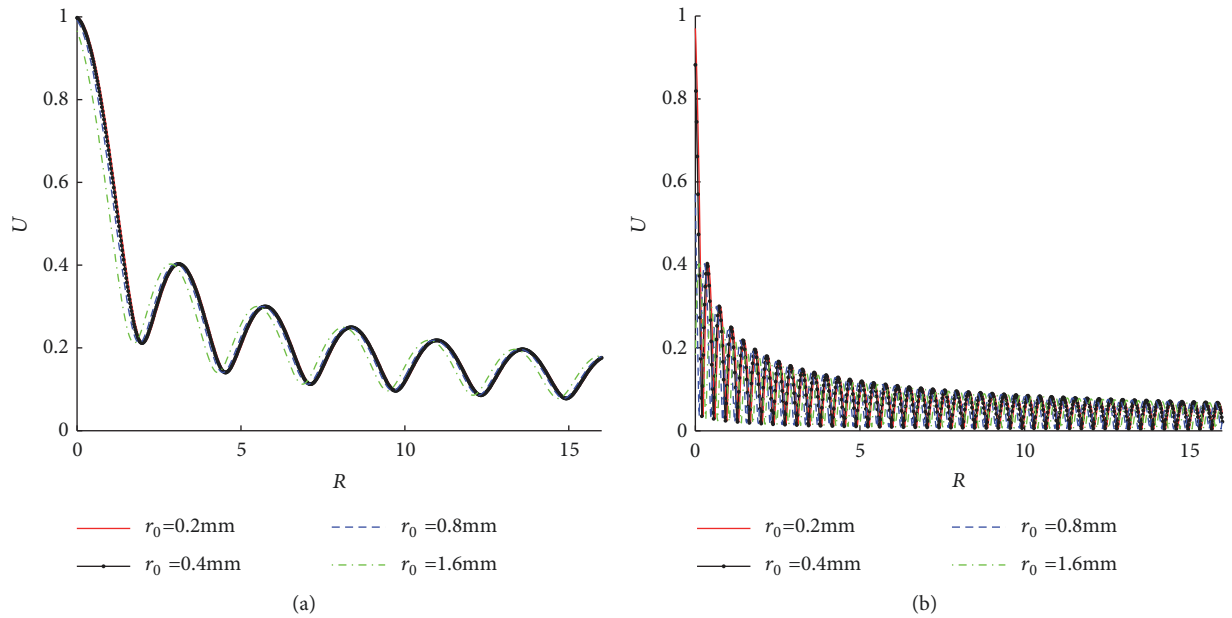

Figure 7: Amplitudes of tissue displacements under different r_0s. (a) $\omega = 2\pi$; (b) $\omega = 16\pi$.

Table 1: R_{thr}s and S_{eff}s under different angular frequencies.

ω	2π	4π	6π	8π	10π	12π	14π	16π
R_{thr}	0.94	0.56	0.36	0.26	0.20	0.16	0.12	0.08
S_{eff}	0.5×0.94	0.5×0.56	0.5×0.36	0.5×0.26	0.5×0.20	0.5×0.16	0.5×0.12	0.5×0.08

stress amplitude in absolute values ($|T_{RZ}|$); it shows the same tendency as $|E_{RZ}|$.

Table 1 lists R_{thr}s and S_{eff}s under different frequencies. Figure 11 shows that there is an approximately linear relationship between R_{thr}s and the reciprocal of the stimulus frequency $1/\omega$s. The same relationship also exists between S_{eff}s and $1/\omega$s.

3.4. Energy Dissipation (ΔE) and Mechanical Quality Factor (Q) under Different Frequencies. Figure 12 shows ΔE and Q under different frequencies. Figure 12(a) shows that ΔE is larger and more intensified around the needle at high frequencies than that at low frequencies. For the mechanical quality factor Q, a nearly linear relationship between Qs and the stimulus frequencies can be found (shown in Figure 12(b)). This means that energy storage ratio increases with the increase of stimulus frequency, and the tissue demonstrates more "elastic" at high frequencies.

4. Discussion

Langevin et al. claimed that acupuncture manipulation would lead to tissue displacement and generate a mechanical stress field [10]. This phenomenon is well demonstrated in our simulation. Moreover, the local displacement, strain, stress, and energy near the acupoint (or the needle) have been quantitively analyzed. The characteristics of the tissue displacement are concluded as (1) it is larger at low frequencies (see Figure 8) given other conditions the same (the needle movement u_0 and the material properties, etc.), and (2), the displacement will decay more slowly and extend relatively further from the needle at low frequencies (see Figure 5).

Main characteristics in the mechanical process of acupuncture are the stimulus amplitude (u_0) and the angular frequency (ω). However, there is a lack of consistency of these characteristics. Wang XM pointed out that mechanical information can only influence nearer region of the acupoint [17]. According to our simulation, the resultant tissue displacement is nearly proportional to u_0 (see Figure 6(a)). It is also shown that the displacement, strain, and stress under low frequency stimulus decay more slowly than those under high frequency (see Figures 8–10). These results indicate that the mechanical information (displacement, strain, and stress) can propagate further under low frequency stimulus. Figure 13 shows the characteristic curves of different acupuncturists, where significant differences in u_0 and ω can be found, but u_0 is larger at high frequencies; thus u_0/ω tends to be constant [18]. Figure 11(a) shows that there is nearly an inverse relationship between R_{thr}s and ωs, or $R_{thr} = k/\omega$, where k is a constant. Given $R = r/u_0$, then the radius of the effective influence area $r_{thr} = u_0 \times R_{thr} = u_0 \times k/\omega = k(u_0/\omega)$. Thus a constant u_0/ω is equivalent to a constant r_{thr}; therefore, to get good acupuncture effect, a sufficient area of tissue should be deformed, which may be an alternative interpolation of acupuncture sensations in the mechanical viewpoint. However, our model is not able to figure out what "sufficient area" should be, which requires further

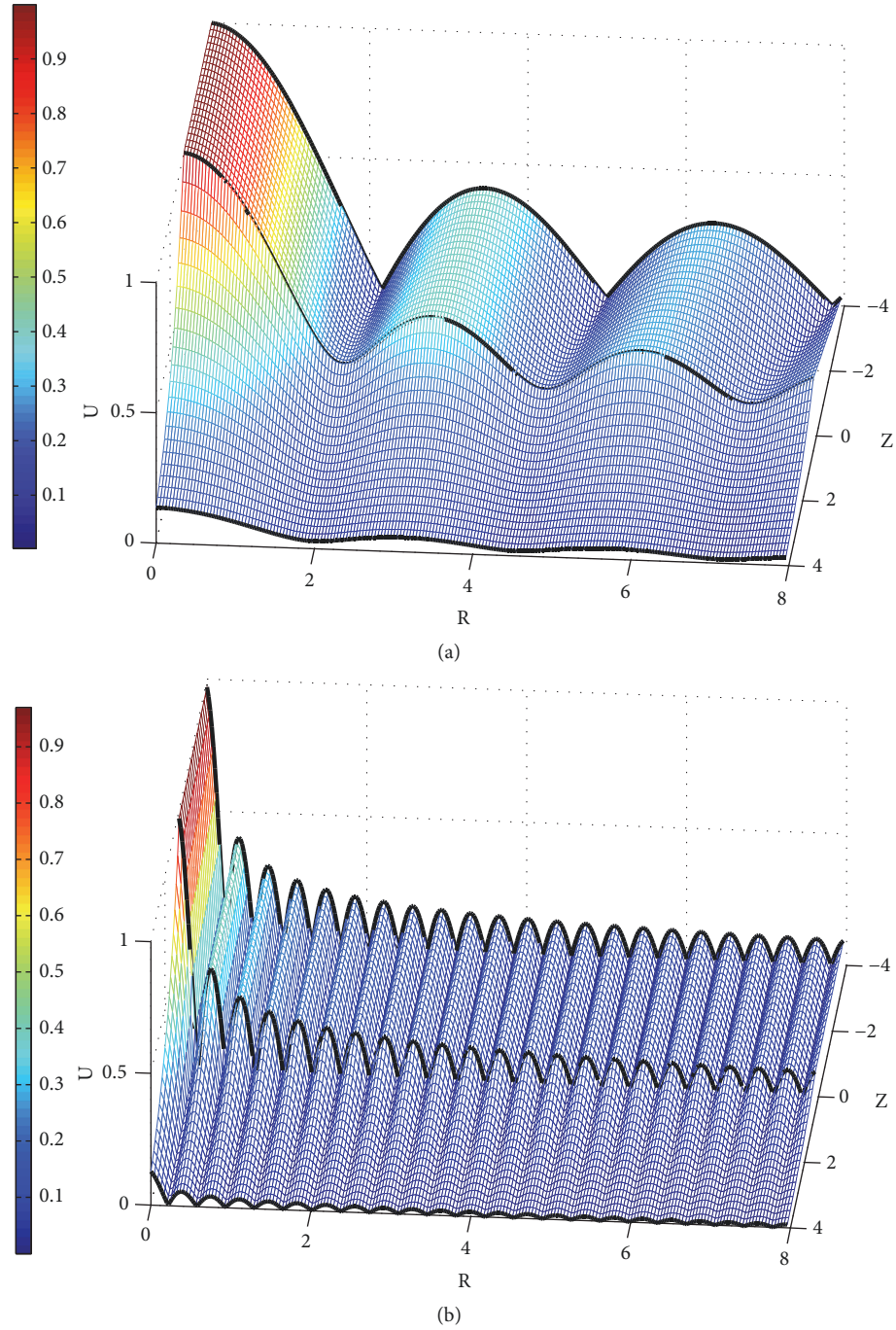

FIGURE 8: Amplitudes of tissue displacements; the black lines represent the displacement at $Z = -L_0/u_0 = -4$, $Z = 0$ and $Z = L_0/u_0 = 4$. (a) $\omega = 2\pi$; (b) $\omega = 16\pi$.

experimental research. But suggestions on achieving mechanical sensations can be made. Since needle movement is a damage process to the tissue and slip between the needle movement and tissue movement may occur at large u_0 (we suppose there is no slip because of small u_0), thus u_0 is limited. Therefore, to achieve better effect (larger effective influence region), low frequency stimulus is a good choice. It was reported that the frequency of acupuncture sensations is concentrated at low frequency [18]. Ding et al. reported the mean frequency to achieve acupuncture sensations by experienced acupuncturists is 1.2 Hz [19].

Figure 7 shows that needle diameter has no effect on displacement. Li et al. reported needling of different diameters induced the consistent change of fascial connective tissues and collagenous fiber arrangement [20]. Figures 9 and 10 show that strain and stress decay quickly under the needle

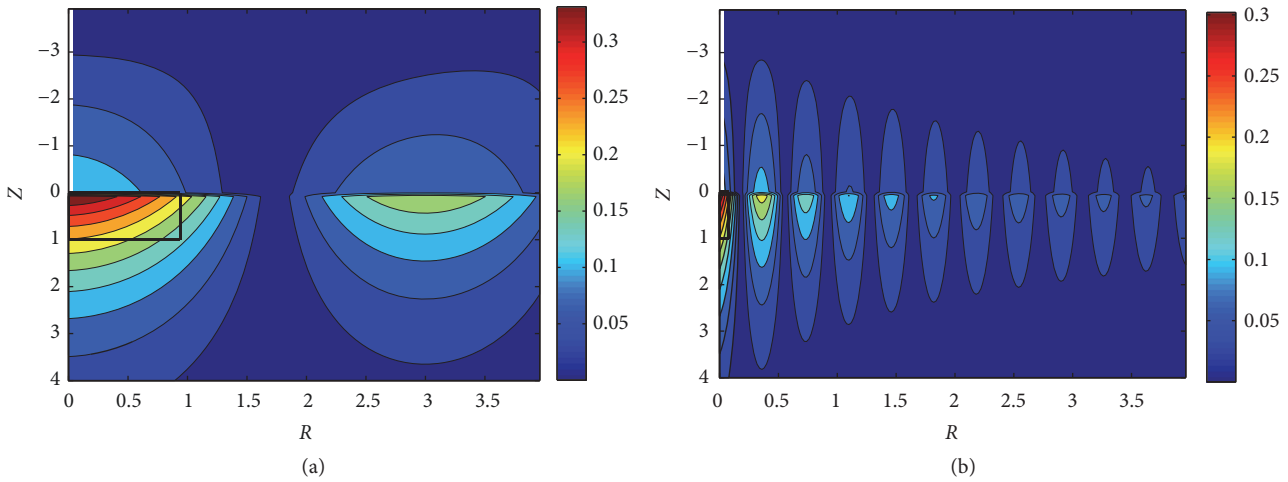

FIGURE 9: Contour lines of $|E_{RZ}|$ in the tissue; the white lines at $r \longrightarrow 0 \cap -4 \leq Z \leq 0$ represent the needle; the black rectangles represent the approximate area where $|E_{RZ}| > 0.2$. (a) $\omega = 2\pi$; (b) $\omega = 16\pi$.

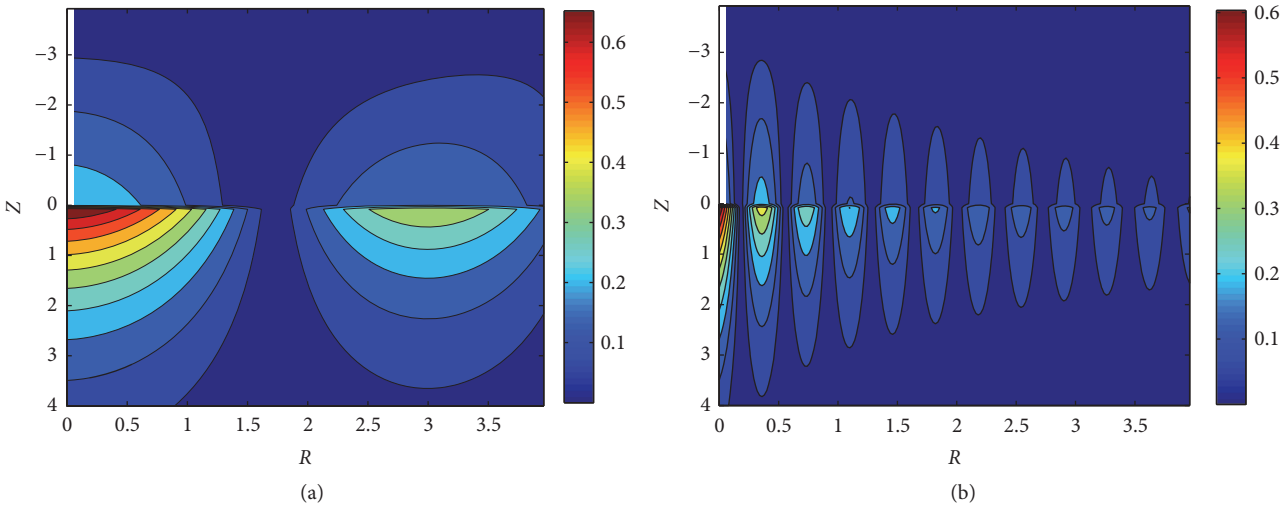

FIGURE 10: Contour lines of $|T_{RZ}|$ in the tissue, the white lines at $R \longrightarrow 0 \cap -4 \leq Z \leq 0$ represent the needle. (a) $\omega = 2\pi$; (b) $\omega = 16\pi$.

tip. That means the needle must be inserted into the right depth (about 2 cm in lower limbs) and position (π/ω cm around the acupoint in our simulation) to induce enough strain and stress. A survey showed that acupuncturists think deep insertion was easier to induce acupuncture sensations than shallow insertion [21].

Because of the limitation of experimental means, it is impossible to measure tissue strain and stress in vivo, tissue displacement, or the stress on the needle are exploited to infer the tissue strain [22]. But there is a complicated relationship between strain and displacement; it is controversial to infer stress field without considering needle frequency. Our model predicted the relationship between the main deformation areas and frequencies (see Figure 11). But there is no agreement on the threshold of $|E_{RZ}|$ to achieve acupuncture effect and tissue is more complicated (anisotropy, nonlinearity) than our model [23]; further experiments are required to testify the results.

Figure 12(a) shows that energy dissipation is relatively small under low frequency compared with that under high frequency; Figure 10(b) shows that there is a linear relationship between mechanical quality factors and frequencies. Obviously, a high energy is required to maintain a high frequency manipulation.

5. Conclusion

In this study, we have illustrated that lifting-thrusting needle will lead to tissue displacements and generate a mechanical stress field. The displacement correlated with needle frequency and decayed more slowly under low frequency than that under high frequency. Strain and stress correlated with frequency too, and there exists an inverse relationship between the main deformation areas and frequencies. Energy dissipation is also affected by frequency. This is a preliminary study of mechanical effects of acupuncture

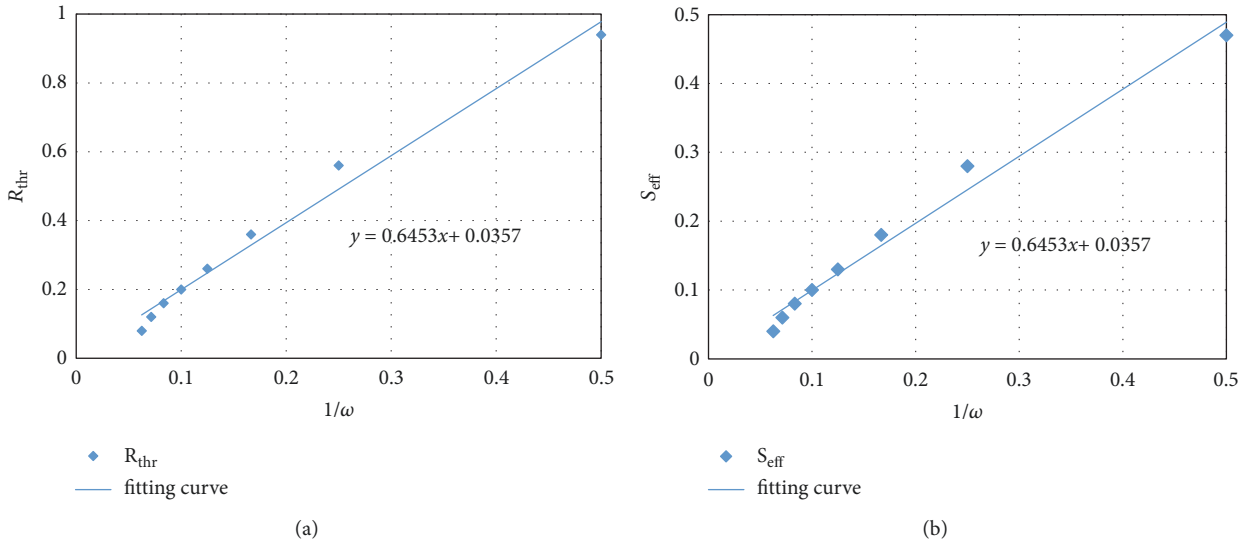

FIGURE 11: Relationship between R_{thr}s and S_{eff}s on one side and $1/\omega$s on the other. Diamonds represent calculating results and blue lines represent the fitting curve.

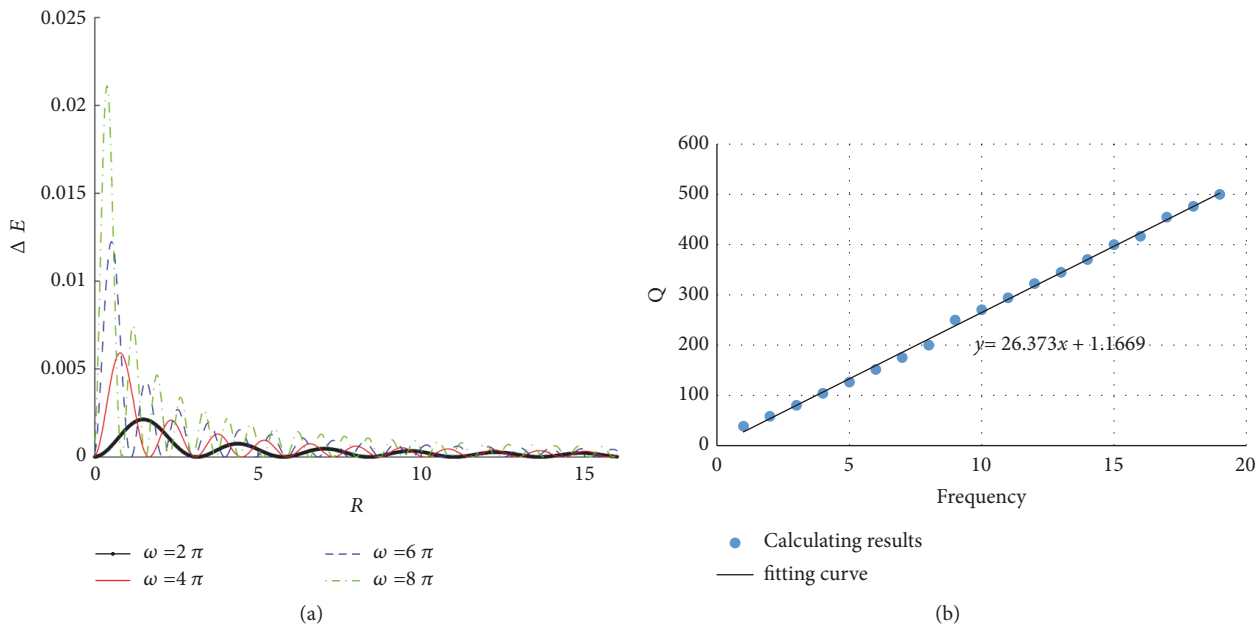

FIGURE 12: ΔE and Q under different frequencies. (a) ΔE at $Z = 0$; (b) Q.

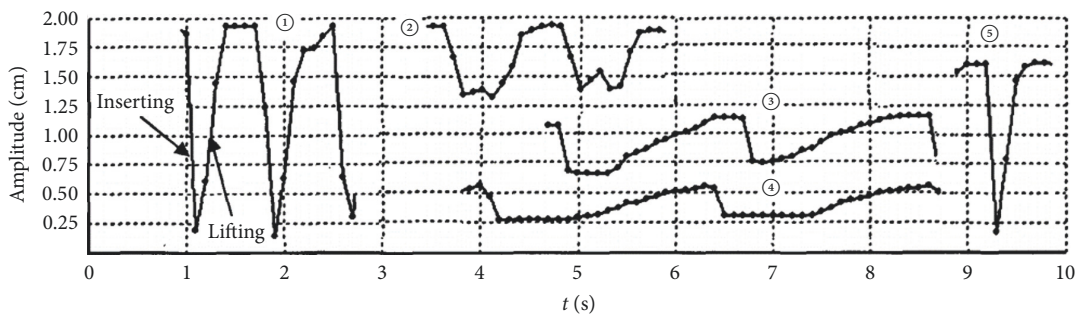

FIGURE 13: Characteristic curves of five professional acupuncturists.

manipulation, isotropy, and quasi-linear viscoelastic theory adopted to simplify soft tissue, while Fox et al. observed anisotropic tissue motion induced by acupuncture [24]. Our results may reflect local effects around the needle; anisotropy must be considered if we study the mechanical information propagation in the tissue.

Data Availability

The data used to support the findings of this study are included within the article. We declared that materials described in the manuscript, including all relevant raw data, will be freely available to any scientist wishing to use them for noncommercial purposes, without breaching participant confidentiality.

Disclosure

This article does not contain any studies with human participants or animals performed by any of the authors.

Conflicts of Interest

The authors declare that they have no conflicts of interest.

Acknowledgments

This study was funded by National Natural Science Foundation of China (81574053 and 81473750) and Shanghai Key Laboratory of Acupuncture Mechanism and Acupoint Function (14DZ2260500).

References

[1] NIH. Acupuncture. in Consensus Development Conference Statement. 1997, https://consensus.nih.gov/1997/1997acupuncture107html.htm:.

[2] L. Fei, G. H. Ding, and E. Y. Chen, "Research progress in physical basis and functional characterization of meridians," in *WHO Report consultation meeting on traditional and modern medicine: harmonizing the two approaches*, Manila, Philippines, 2000.

[3] M. F. Luo, X. T. Dong, X. J. Somg, J. Jin, J. L. Zhann, and Y. Han, "Study on the dynamic compound structure composed of mast cells, blood vessels, and nerves in rat acupoint," *Evidence-Based Complementary and Alternative Medicine*, vol. 2013, Article ID 160651, 4 pages, 2013.

[4] Y. L. Goh, C. E. Ho, and B. Zhao, "Acupuncture and depth: future direction for acupuncture research," *Evidence-based Complementary and Alternative Medicine*, vol. 2014, Article ID 871217, 5 pages, 2014.

[5] H. M. Langevin, D. L. Churchill, and M. J. Cipolla, "Mechanical signaling through connective tissue: a mechanism for the therapeutic effect of acupuncture," *The FASEB Journal*, vol. 15, no. 12, pp. 2275–2282, 2001.

[6] H. M. Langevin, "The science of stretch," *The Scientist*, vol. 27, no. 5, p. 32, 2013.

[7] X. Yu, G. Ding, H. Huang, J. Lin, W. Yao, and R. Zhan, "Role of collagen fibers in acupuncture analgesia therapy on rats," *Connective Tissue Research*, vol. 50, no. 2, pp. 110–120, 2009.

[8] A. Mvogo, G. H. Ben-Bolie, and T. C. Kofané, "Energy transport in the three coupled α−polypeptide chains of collagen molecule with long-range interactions effect," *Chaos*, Article ID 063115, pp. 1–9, 2015.

[9] C. Stecco, C. Tiengo, and A. Stecco, "Fascia redefined: anatomical features and technical relevance in fascial flap surgery," *Surgical and Radiologic Anatomy*, vol. 35, no. 5, pp. 369–376, 2013.

[10] H. M. Langevin, E. E. Konofagou, G. J. Badger et al., "Tissue displacements during acupuncture using ultrasound elastography techniques," *Ultrasound in Medicine & Biology*, vol. 30, no. 9, pp. 1173–1183, 2004.

[11] Y. Deleuze, M. Thiriet, and T. W. Sheu, "Modeling and simulation of the interstitial medium deformation induced by the needle manipulation during acupuncture," *Communications in Computational Physics*, vol. 18, no. 04, pp. 850–867, 2015.

[12] M. Thiriet, Y. Deleuze, and T. W. Sheu, "A biological model of acupuncture and its derived mathematical modeling and simulations," *Communications in Computational Physics*, vol. 18, no. 04, pp. 831–849, 2015.

[13] W. Yao, Y. Yu, and G. Ding, "A hybrid method to study the mechanical information induced by needle rotating," *Mathematical Methods in the Applied Sciences*, vol. 41, no. 15, pp. 5939–5950, 2018.

[14] S. Nicolle, J. Decorps, B. Fromy, and J. Palierne, "New regime in the mechanical behavior of skin: strain-softening occurring before strain-hardening," *Journal of the Mechanical Behavior of Biomedical Materials*, vol. 69, pp. 98–106, 2017.

[15] L. Wang, G. H. Tao, M. D. Tao, and G. H. Ding, "The calculation of energy distribution based on two respective techniques of acupuncture therapy," *Journal of Medical Biomechanics*, vol. 18, no. 4, pp. 195–201, 2003 (Chinese).

[16] Y. C. Fung, *Mechanical Properties of Living Tissues*, Springer, Berlin, Germany, 1993.

[17] X.-M. Wang, "Lifting-thrusting and rotating manipulations :a comparison on energy input," *Chinese Acupuncture & Moxibustion*, vol. 31, no. 1, pp. 71–74, 2011 (Chinese).

[18] T.-Y. Liu, L. Kuai, H.-Y. Yang, and M. Gao, "Preliminary research on the standardization of acupuncture manipulation," *Chinese Acupuncture & Moxibustion*, vol. 28, no. 5, pp. 356–358, 2008.

[19] G. H. Ding, X. Y. Shen, J. H. Dai et al., "The difference of acupuncture manipulation frequencies of lifting-thrusting and twirling-rotating at deqi and non-deqi," *Chinese Acupuncture & Moxibustion*, vol. 22, no. 10, pp. 679–681, 2002 (Chinese).

[20] C. Li, B. Chen, T. H. Hu, and L. Chen, "Effects of acupuncture with different filiform needles on tissues," *Chinese Acupuncture & Moxibustion*, vol. 35, no. 8, pp. 801–805, 2015 (Chinese).

[21] Y. L. Ren, T. P. Guo, H. B. Du et al., "A survey of the practice and perspectives of chinese acupuncturists on deqi," *Evidence-Based Complementary and Alternative Medicine*, vol. 2015, Article ID 684708, 8 pages, 2015.

[22] Y. S. Lee, W. M. Jung, I. S. Lee et al., "Visualizing motion patterns in aupuncture manipulation," *Journal of Visualized Experiments*, vol. 113, Article ID e54213, pp. 1–7, 2016.

[23] L. Falland-Cheung, M. Scholze, P. F. Lozano et al., "Mechanical properties of the human scalp in tension," *Journal of the Mechanical Behavior of Biomedical Materials*, vol. 84, pp. 188–197, 2018.

[24] J. R. Fox, W. Gray, C. Koptiuch, G. J. Badger, and H. M. Langevin, "Anisotropic tissue motion induced by acupuncture needling along Intermuscular connective tissue planes," *The Journal of Alternative and Complementary Medicine*, vol. 20, no. 4, pp. 290–294, 2014.